

Upward Shift of the Atmospheric General Circulation under Global Warming: Theory and Simulations

MARTIN S. SINGH AND PAUL A. O'GORMAN

Massachusetts Institute of Technology, Cambridge, Massachusetts

(Manuscript received 30 November 2011, in final form 8 May 2012)

ABSTRACT

Many features of the general circulation of the atmosphere shift upward in response to warming in simulations of climate change with both general circulation models (GCMs) and cloud-system-resolving models. The importance of the upward shift is well known, but its physical basis and the extent to which it occurs coherently across variables are not well understood. A transformation is derived here that shows how an upward shift of a solution to the moist primitive equations gives a new approximate solution with higher tropospheric temperatures. According to the transformation, all variables shift upward with warming but with an additional modification to the temperature and a general weakening of the pressure velocity. The applicability of the vertical-shift transformation is explored using a hierarchy of models from adiabatic parcel ascents to comprehensive GCMs. The transformation is found to capture many features of the response to climate change in simulations with an idealized GCM, including the mid- and upper-tropospheric changes in lapse rate, relative humidity, and meridional wind. The transformation is less accurate when applied to simulations with more realistic GCMs, but it nonetheless captures some important features. Deviations from the simulated response are primarily due to the surface boundary conditions, which do not necessarily conform to the transformation, especially in the case of the zonal winds. The results allow for a physical interpretation of the upward shift in terms of the governing equations and suggest that it may be thought of as a coherent response of the general circulation of the mid- and upper troposphere.

1. Introduction

A robust feature of simulations of climate change in a variety of different models is a tendency for the atmospheric circulation to shift upward as the climate warms. Studies with general circulation models (GCMs) forced with increasing greenhouse gas concentrations have found an upward shift in the static stability profile (Kushner et al. 2001), transient kinetic energy and momentum flux (Lorenz and DeWeaver 2007), relative humidity (Sherwood et al. 2010), large-scale condensation rate (O'Gorman and Schneider 2008), and cloud fraction (Mitchell and Ingram 1992). Studies with cloud-system-resolving models have also found upward shifts in response to warming, including upward shifts in the vertical velocities and distributions of cloud water and ice as the sea surface temperature is increased (Tompkins and Craig 1999; Kuang and Hartmann 2007; Muller et al. 2011).

One of the aims of this paper is to further document the upward shift in a wide range of variables and simulations. As a first example, Fig. 1 shows the changes in zonal-mean cloud fraction in a climate-change simulation with the Geophysical Fluid Dynamics Laboratory (GFDL) Coupled Model version 2.1 (CM2.1), and the corresponding changes obtained by an upward shift based on the climatology of cloud fraction from the same model. We define the upward shift as a transformation in pressure coordinates so that $C'(p) = C(\beta p)$, where p is the pressure, C is the climatology of cloud fraction, and C' is the estimate of the cloud fraction in the warmer climate. The parameter $\beta = 1.12$ controls the magnitude of the shift; it is set based on the temperature changes simulated by the model (see section 5). The upward shift reproduces many of the features of the changes in cloud fraction simulated by the model, especially in the tropics and subtropics.

Mechanisms have previously been proposed to explain such upward shifts in clouds and certain other aspects of the general circulation as the climate is warmed. Artificially raising the tropopause in simulations with

Corresponding author address: Martin S. Singh, 77 Massachusetts Ave., Bldg. 54-1715, Cambridge, MA 02139.
E-mail: mssingh@mit.edu

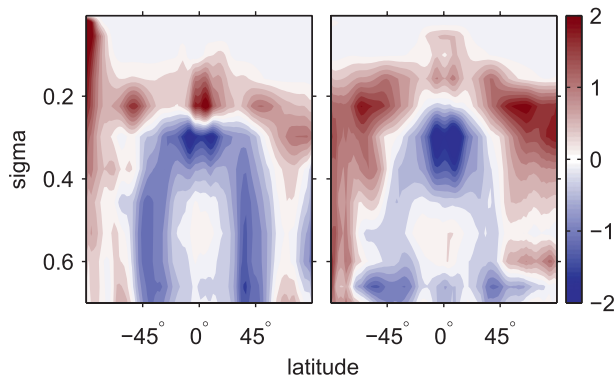


FIG. 1. (left) Changes in zonal- and time-mean cloud fraction (%) between the last 20 years of the twentieth and twenty-first centuries as simulated by GFDL CM2.1 under SRESA1b (Nakićenović and Swart 2000). (right) Changes in the same statistic that result from an upward shift of the climatology of the last 20 years of the twentieth century (see text for details). The vertical coordinate is σ (pressure normalized by surface pressure). All changes shown are normalized by the change in global-mean surface air temperature (K).

a dry idealized GCM results in a shift of the zonal wind and eddy kinetic energy fields upward and poleward, similar to the changes that occur in comprehensive models forced with increases in greenhouse gas concentrations (Lorenz and DeWeaver 2007). This suggests that increases in the height of the tropopause could be an important driver of shifts in the wind field. An upward shift in tropical cloud properties as the surface is warmed has been attributed to the constraint on the temperature structure to remain close to neutral for moist convection (Tompkins and Craig 1999). At a higher SST, the temperature remains pinned to a warmer moist adiabat, while the cloud features occur in the same temperature range. Since isotherms move upward as the climate is warmed, an upward shift in the profile results. The Fixed Anvil Temperature (FAT) hypothesis of Hartmann and Larson (2002) suggests that convective anvil clouds, in particular, must remain at approximately the same temperature as the climate changes. This is because the vertical profile of heating in tropical convection is strongly constrained by the radiative cooling in clear-sky regions. Since the dominant longwave emitter in the troposphere is water vapor, its distribution essentially determines the distribution of radiative cooling. The dependence of saturation vapor pressure on temperature then ensures that the height to which cooling reaches, and thus the height of cloud tops and the circulation, must shift upward as temperature increases.

We have, therefore, some understanding of why certain atmospheric properties might shift upward with warming (at least in the tropics or near the tropopause). The need for an upward extension of the circulation with

warming follows from the need to balance the upward extension of the radiative cooling rate as water vapor concentrations increase, and an upward shift may provide a consistent response of the circulation to the extent that latent heating rates and cloud properties also shift upward. An upward shift cannot completely describe the response of the general circulation to warming because of the need to satisfy the surface boundary conditions, but it may provide a reasonable approximation to it sufficiently far from the lower boundary.

An advantage of viewing the atmospheric response to climate change in terms of shifts of the circulation is that one can then use observations of the general circulation in the present climate to inform predictions of its behavior in a different climate. Motivated by this, and the ubiquity of the upward-shift response in model simulations, we seek to provide a more general theoretical basis for these vertical shifts that applies to all dynamic and thermodynamic variables. We construct a transformation based on the moist primitive equations that allows for the circulation to shift vertically while maintaining conservation of energy, water, and momentum. Thus, based on the governing equations and information about the current climate, we construct an estimate of the changes in the general circulation as the climate is warmed or cooled. The transformation may be viewed as giving the vertical structure of the response to climate change, but not the horizontal shifts in the circulation.¹ We do not consider cloud properties in the transformation so as to avoid dealing with the complexities of cloud microphysics, but we do consider related large-scale quantities such as the statistics of relative humidity and vertical velocity; the changes in cloud fraction shown in Fig. 1 suggest that the theory could be extended to include changes in the cloud field.

We will show that the governing equations require that the vertical-shift transformation is not purely a vertical shift in the case of temperature or pressure (vertical) velocity. In addition to shifting upward with warming, the pressure velocity also decreases in magnitude, implying a decrease in strength of the overturning circulation. While it is not immediately apparent that the decrease in circulation strength is related to the upward shift, the transformation implies that the two occur in tandem. A slowing down of the overturning circulation with warming has previously been related to the different rates of increase of specific humidity and precipitation in response to a given forcing (e.g., Held

¹ The horizontal and vertical shifts of the circulation may be linked (e.g., Lorenz and DeWeaver 2007), and a decomposition into horizontal and vertical shifts is necessarily an idealization.

and Soden 2006). While the accuracy of simple scaling arguments for the strength of the overturning circulation has been questioned (Schneider et al. 2010; Merlis and Schneider 2011), many model simulations do show a decrease in magnitude of the resolved-scale pressure velocity in the tropics in their response to greenhouse-gas-induced warming (Knutson and Manabe 1995; Vecchi and Soden 2007).

We begin by deriving the vertical-shift transformation from the governing equations (section 2); a summary of the transformation is given by Eqs. (13a)–(13g). We then apply the transformation to simulations of warming in a number of models of varying complexity. Our aims are to determine the conditions under which it provides a good approximation to the response of the atmosphere to warming and to better interpret changes in more comprehensive models. We first demonstrate the ability of the transformation to reproduce pseudoadiabatic parcel ascents initialized with different temperatures (section 3). We also consider an idealized aquaplanet GCM in which the radiative cooling is parameterized so as to conform to the transformation (section 4). We then examine simulations performed for the World Climate Research Programme third Coupled Model Intercomparison Project (CMIP3) and evaluate the extent to which the simple transformation reproduces the simulated response to greenhouse gas and other forcings in comprehensive GCMs (section 5). Last, we summarize our results and discuss their implications (section 6).

2. Derivation of the transformation

a. Winds and geopotential

We work with the primitive equations in pressure coordinates and begin by considering the transformation of the winds and geopotential. The inviscid zonal momentum equation is given by

$$\begin{aligned} \frac{\partial u}{\partial t} + \frac{u}{a \cos \phi} \frac{\partial u}{\partial \lambda} + \frac{v}{a} \frac{\partial u}{\partial \phi} + \omega \frac{\partial u}{\partial p} \\ = -\frac{1}{a \cos \phi} \frac{\partial \Phi}{\partial \lambda} + 2\Omega v \sin \phi + \frac{uv \tan \phi}{a}, \end{aligned}$$

where u and v are the zonal and meridional velocities, ω is the pressure velocity, a is the radius of the earth, Ω is the rotation rate, and Φ is the geopotential. All fields are functions of latitude ϕ , longitude λ , pressure p , and time t . Given a solution to the equations with zonal wind $u(\lambda, \phi, p, t)$ and meridional wind $v(\lambda, \phi, p, t)$, we define transformed winds (denoted by a prime) by setting

$$u'(\lambda, \phi, p, t) = u(\lambda, \phi, \beta p, t), \quad (1a)$$

$$v'(\lambda, \phi, p, t) = v(\lambda, \phi, \beta p, t). \quad (1b)$$

The transformation parameter β governs the magnitude of the rescaling in pressure; it will subsequently be taken to be close to unity. For values of $\beta > 1$, the circulation is shifted upward by the transformation. By substitution, we find that the transformed solution satisfies the zonal momentum equation if we also define transformed pressure velocity and geopotential fields as

$$\omega'(\lambda, \phi, p, t) = \frac{\omega(\lambda, \phi, \beta p, t)}{\beta}, \quad (2a)$$

$$\Phi'(\lambda, \phi, p, t) = \Phi(\lambda, \phi, \beta p, t) + \Lambda(\beta p), \quad (2b)$$

for an arbitrary function of pressure $\Lambda(p)$. Similar considerations hold for the meridional momentum and continuity equations. Thus, for any solution of the horizontal momentum and continuity equations, we can find a corresponding vertically shifted solution defined by (1) and (2) that depends on the parameter β . The perturbation to the geopotential, $\Lambda(p)$, is a further degree of freedom by which the solution may be altered; its functional form will be constrained by the thermodynamic and hydrostatic equations.

b. Temperature

The hydrostatic equation may be written approximately as

$$T = -\frac{p}{R} \frac{\partial \Phi}{\partial p}, \quad (3)$$

where T is the temperature and R is the gas constant for air.² Substitution of (2b) into (3) implies that the transformed temperature field must satisfy

$$T'(\lambda, \phi, p, t) = T(\lambda, \phi, \beta p, t) - \Delta T(\beta p), \quad (4)$$

where we have introduced

$$\Delta T(p) = \frac{p}{R} \frac{d\Lambda}{dp}. \quad (5)$$

To determine the form of ΔT we enforce the requirement that the transformed solution satisfies the thermodynamic equation

² Here, and for the rest of the derivation, we neglect the effects of water vapor on density and specific heat capacity, we take the latent heat of vaporization to be constant, and we neglect ice processes.

$$c_p \Pi(p) \frac{D\theta}{Dt} = -L_v \frac{Dq}{Dt} + Q_{\text{rad}}, \quad (6)$$

where $\theta = T/\Pi$ is the potential temperature, $\Pi(p) = (p/p_0)^{R/c_p}$ is the Exner function, q is the specific humidity, L_v is the latent heat of vaporization, c_p is the specific heat capacity of air, and Q_{rad} the radiative heating rate. To begin with, consider the simple case of unsaturated, adiabatic motion, in which the right-hand side of (6) vanishes. The thermodynamic equation reduces to the conservation of potential temperature, and any constant may be added to the potential temperature while still satisfying the equation. Hence, the transformed temperature (4) will satisfy the thermodynamic equation in this dry-adiabatic case if it has the form

$$T'(\lambda, \phi, p, t) = T(\lambda, \phi, \beta p, t) - \Delta\theta \Pi(\beta p), \quad (7)$$

where $\Delta\theta$ is a constant, which may be varied independently of β . The freedom to independently rescale pressure by β in the dry primitive equations does not hold in the moist primitive equations because the water vapor pressure then enters (Garner et al. 2007).³ As a result, the parameters $\Delta\theta$ and β are no longer independent in a moist atmosphere, as we shall now see.

c. Moist processes

Returning to the thermodynamic equation (6), we consider the transformation of the latent heating term [the first term on the rhs of (6)]. We set $\Delta T = \Delta\theta \Pi$, with $\Delta\theta$ constant, as in the dry case, so that dry adiabatic motions still transform correctly. For the latent heating term to transform correctly, we must also require that the specific humidity shifts vertically according to

$$q'(\lambda, \phi, p, t) = q(\lambda, \phi, \beta p, t). \quad (8)$$

We prescribe that both relative humidity \mathcal{R} and saturation specific humidity q_s are similarly vertically shifted so that (8) is satisfied and the equation governing conservation of water vapor,

$$\frac{Dq}{Dt} = -c, \quad (9)$$

is also satisfied, assuming that the net condensation rate (c) is a local function of variables such as the relative humidity, specific humidity, and winds.

The saturation specific humidity q_s is a thermodynamic function of pressure and temperature, and so its transformation depends on the transformation of temperature. For simplicity, we approximate q_s as

$$q_s = \frac{\epsilon e_s(T)}{p}, \quad (10)$$

where e_s is the saturation vapor pressure and ϵ is the ratio of gas constants for dry air and water vapor, although the final result does not depend on this approximation. We assume a small upward shift ($\beta - 1 \ll 1$) and that ΔT is small enough to allow linearization of the dependence of saturation vapor pressure on temperature. Substituting the transformed temperature (7) into (10) and performing this linearization, we find that

$$q'_s(p) = \beta q_s(\beta p) \left[1 - \frac{L_v}{R_v T(\beta p) \theta(\beta p)} \Delta\theta \right],$$

where R_v is the gas constant for water vapor, the Clausius–Clapeyron equation has been used, and the dependence on horizontal coordinates and time has been suppressed for brevity. Thus, $q'_s(\lambda, \phi, p, t) = q_s(\lambda, \phi, \beta p, t)$ holds when

$$\Delta\theta = \left(\frac{\beta - 1}{\beta} \right) \left(\frac{R_v}{L_v} \right) T\theta, \quad (11)$$

which will only be strictly satisfied if the product $T\theta$ is constant since both β and $\Delta\theta$ must not vary in space or time. In practice, the relation (11) will be most important in regions in which latent heating is a significant term in the thermodynamic equation. In the low to mid-troposphere, where latent heating is important, temperature decreases with height and potential temperature increases with height with the result that for atmospheric profiles typical of the earth's atmosphere, the function $T\theta$ does not vary by more than 10% between the surface and upper troposphere. We will further discuss the approximation of constant $T\theta$ and the errors it introduces in section 3.

d. Radiation

The vertical-shift transformation of the thermodynamic equation (6) is only valid if the radiative cooling rate in the atmosphere is also shifted vertically,

$$Q'_{\text{rad}}(\lambda, \phi, p, t) = Q_{\text{rad}}(\lambda, \phi, \beta p, t). \quad (12)$$

The extent to which the radiative cooling rate shifts upward with warming has been discussed to some extent in previous studies (Hartmann and Larson 2002; Ingram 2010). The rate of radiative cooling in the free troposphere does not vary strongly in the vertical (e.g.,

³ The transformation presented here is not the same as the hypohydrostatic rescaling outlined in Garner et al. (2007). The vertical-shift transformation applies to the hydrostatic primitive equations, whereas the hypohydrostatic rescaling only alters the equations in the nonhydrostatic regime.

Dopplack 1972; Hartmann et al. 2001), and thus the most important issue is whether the upper limit of the region of strong radiative cooling shifts vertically in accordance with the transformation. One way for this to occur is if the radiative cooling rate declines at a level determined by the distribution of specific humidity (specific humidity and radiative cooling shift vertically in the same way according to the transformation), in a similar way to the FAT hypothesis mentioned in the introduction (Hartmann and Larson 2002). Simulations with cloud-system-resolving models have shown that the tropical cloud distribution does follow the FAT hypothesis, even with changes to the ozone distribution and CO₂ concentration (Kuang and Hartmann 2007). In the extratropics, however, there is less justification for this simplified view of the radiative response of the atmosphere.

e. Boundary conditions

The surface boundary conditions are not satisfied in detail by the transformation. We can, however, ensure that the boundary conditions on geopotential and temperature are satisfied to some extent. An immediate problem is that, for a finite upward shift ($\beta > 1$), there is a region near the surface in which the transformed solution is not defined, as it refers to the original solution below the surface, and the transformed solution must be extrapolated. This issue is less problematic the smaller the climate change, and it does not arise for the downward shift associated with a cooling climate. More importantly, because we only expect the transformed solution to be valid above the boundary layer (the boundary layer tendencies are strongly tied to the surface and cannot shift upward),⁴ the boundary conditions should be applied at or above the top of the boundary layer rather than at the surface.

We begin with the boundary condition on the geopotential Φ and impose the requirement that the mass of the free troposphere is unchanged by the transformation. Since only the first derivative of $\Lambda(p)$ is constrained by the combination of (5) and (11), we can introduce an integration constant $\Delta\Phi$ to set the geopotential near the top of the boundary layer. The remaining parameters in the transformation, β and $\Delta\theta$, are related by (11) and thus may be used to satisfy only one boundary condition, which

we take to be temperature. (In practice, we will choose β using a least squares criterion based on global temperature changes above the boundary layer.) The need to satisfy the boundary conditions at all positions and times introduces a further approximation since the transformation parameters must be constant. The inability of the transformation to satisfy the boundary conditions on wind and relative humidity will be seen to be the largest contributor to the mismatch between the responses to climate change given by the transformation and the simulations in sections 4 and 5.

f. Summary of transformation

The result of the preceding derivation is that, for any solution to the moist primitive equations, we can find a family of new solutions using the following transformation:

$$u'(\lambda, \phi, p, t) = u(\lambda, \phi, \beta p, t), \quad (13a)$$

$$v'(\lambda, \phi, p, t) = v(\lambda, \phi, \beta p, t), \quad (13b)$$

$$\omega'(\lambda, \phi, p, t) = \frac{\omega(\lambda, \phi, \beta p, t)}{\beta}, \quad (13c)$$

$$\Phi'(\lambda, \phi, p, t) = \Phi(\lambda, \phi, \beta p, t) + c_p \Delta\theta \Pi(\beta p) + \Delta\Phi, \quad (13d)$$

$$T'(\lambda, \phi, p, t) = T(\lambda, \phi, \beta p, t) - \Delta\theta \Pi(\beta p), \quad (13e)$$

$$\mathcal{R}(\lambda, \phi, p, t) = \mathcal{R}(\lambda, \phi, \beta p, t), \quad (13f)$$

$$Q'_{\text{rad}}(\lambda, \phi, p, t) = Q_{\text{rad}}(\lambda, \phi, \beta p, t). \quad (13g)$$

The parameter β determines the magnitude of the vertical shift (and is set by the temperature change), $\Delta\Phi$ is used to satisfy the boundary condition on geopotential, and $\Delta\theta$ is given by (11). Figure 2 shows a schematic of how the transformation affects typical profiles of temperature, zonal wind, and pressure velocity. In particular, the temperature and pressure velocity are not simply shifted vertically (as shown by the gray dashed lines), but a pressure-dependent offset is applied to the temperature, and the pressure velocity is decreased in magnitude.

Some further insight is gained by explicitly relating β to the change in temperature. Substituting the expression (11) for $\Delta\theta$ into (13e) and discarding terms on the order of $(\beta - 1)^2$ or higher gives

$$T'(\lambda, \phi, p, t) \simeq T(\lambda, \phi, p, t) + (\beta - 1)p \frac{\partial T}{\partial p} - (\beta - 1) \frac{R_v}{L_v} T^2.$$

Denoting δT as the difference in temperature between the original and warm climate at a fixed pressure level, we have

⁴ Additionally, the derivation assumes an inviscid atmosphere and is not a good approximation in the boundary layer in which small-scale turbulent eddies are dynamically important. While these eddies themselves are governed by the Navier–Stokes equations and could be encapsulated within the transformation, the hydrostatic form of the equations used is more appropriate for large-scale flow. Also, in the case of climate models, small-scale turbulence is often parameterized by schemes that do not respect the equations of motion.

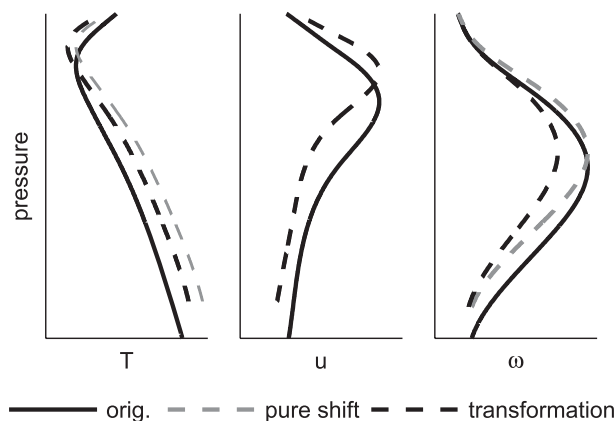


FIG. 2. Schematic of the effect of the transformation on (left) temperature, (middle) zonal wind, and (right) pressure velocity. Solid lines show the original solution and dashed lines show the transformed solution. For comparison, gray dashed lines show a pure upward shift for temperature and pressure velocity neglecting the extra terms introduced by the transformation [see Eqs. (13c) and (13e)].

$$\delta T \simeq (\beta - 1) \left(p \frac{\partial T}{\partial p} - e_s \frac{dT}{de_s} \right),$$

where the Clausius–Clapeyron equation has been used. The sensitivity of the upward shift to temperature change may then be written as

$$\frac{\beta - 1}{\delta T} \simeq [(H_p - H_e)\Gamma]^{-1}, \quad (14)$$

where H_p and H_e are the scale heights for pressure and water vapor, respectively, defined by

$$H_p = -\frac{\partial z}{\partial \ln p},$$

$$H_e = -\frac{\partial z}{\partial \ln e_s},$$

with z the geopotential height and $\Gamma = -\partial T/\partial z$ the lapse rate. Substituting characteristic top-of-boundary layer values of $H_p \simeq 8$ km, $e_s^{-1} de_s/dT \simeq 0.07$ K⁻¹, and $\Gamma \simeq 5$ K km⁻¹, we find that

$$\frac{\beta - 1}{\delta T_{BL}} \approx 0.04 \text{K}^{-1}, \quad (15)$$

where δT_{BL} is the change in temperature at a fixed pressure level near the top of the boundary layer. This value of β is somewhat sensitive to the assumed lapse rate, but it gives a rough sense of the magnitude of vertical shift that may be expected for a given level of warming.

It is also possible to formulate the transformation in geopotential height coordinates (z), in which case the vertical shift becomes more explicit. For example, the transformation of the zonal wind may be written as

$$u'(\lambda, \phi, z, t) = u(\lambda, \phi, z - \Delta z, t),$$

where Δz is the vertical shift in height. The pressure and density fields are shifted up similarly but must also be divided by β . The equivalence of the pressure and height formulations follows from the transformation of the geopotential in (13d). In the case of a dry atmosphere, we can take $\Delta\theta = 0$, and the vertical shift Δz is a constant; the transformation follows from translational invariance and the form of the ideal gas law. In the more general case of a moist atmosphere, the vertical shift Δz varies in the vertical, and it becomes much easier to demonstrate the validity of the transformation using pressure coordinates. We will refer to the transformation as a vertical shift for convenience, even though the magnitude of the vertical shift varies with height and even though the temperature change is not purely a vertical shift.

3. Parcel ascents

We begin the evaluation of the vertical-shift transformation in the simplified setting of idealized parcel ascents in which we only consider temperature and moisture. This approach allows us to examine the effects of the approximation made in the derivation related to the latent heating term in the thermodynamic equation (cf. section 2c).

For a dry-adiabatic parcel ascent or descent, we have that the potential temperature is uniform. Increasing the initial parcel temperature yields a temperature profile with a constant but higher potential temperature. The transformation gives the exact warmer solution by construction regardless of the combination of β and $\Delta\theta$ that is used to match the increase in initial temperature. The requirement that $T\theta$ be constant does not apply because (11) is only required to hold when moisture affects the thermodynamic equation. Thus, the vertical-shift transformation can exactly reproduce a shift to a warmer “climate” in the case of dry-adiabatic displacements.

Moist-adiabatic parcel ascents are a nontrivial test because of the requirement of approximately constant $T\theta$ for the transformed moist thermodynamic budget to be accurate. We evaluate the accuracy of the transformation for pseudoadiabatic parcel ascents. For simplicity we assume a constant latent heat of vaporization and neglect ice processes, consistent with the idealized simulations described in the next section. Figure 3 shows an example of one such ascent for a surface temperature

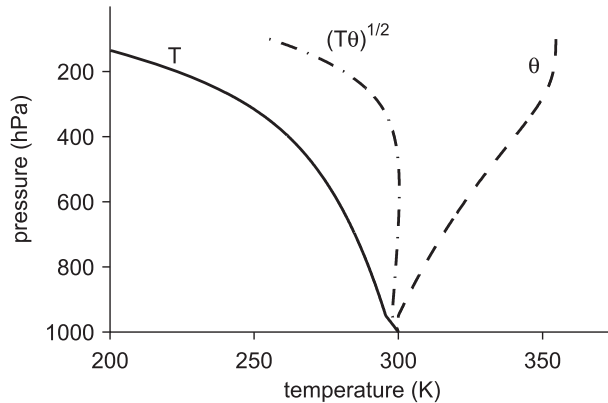


FIG. 3. Pseudoadiabatic parcel ascent with a surface temperature of 300 K and surface relative humidity of 80%. Shown are the temperature T (solid), potential temperature θ (dashed), and their geometric mean $(T\theta)^{1/2}$ (dot dashed).

of 300 K and a surface relative humidity of 80%. The ascents follow a dry adiabat up to saturation, and the air parcels are assumed to remain at saturation for the remainder of the ascent. We choose a surface air temperature characteristic of the tropics because the tropics is where condensation, and thus the constraint of invariant $T\theta$ given by (11), is most important. The product $(T\theta)^{1/2}$ remains roughly constant up to a pressure of ~ 300 hPa, varying by only 2% between the surface and this level, implying that the vertical-shift transformation should work well in this case. Latent heating is weaker at levels above 300 hPa, and the condition of constant $T\theta$ is less dynamically important, although the transformation of specific humidity may still matter for the effect of water vapor on radiative transfer.

We next consider the application of the vertical-shift transformation to the difference in temperature between pseudoadiabatic ascents with surface relative humidities of 80% and surface temperatures of 300 K (the control parcel) and 302 K (the warm parcel). The vertical-shift transformation is applied to the control parcel so as to reproduce the warm parcel ascent (Fig. 4a), and the implied difference in temperature is compared with the actual difference in temperature between the two parcel ascents (Fig. 4b). The value of β used for the vertical-shift solution is determined using a least squares criterion in which we minimize the nondimensional error function

$$E^2 = \frac{\overline{(T_w - T_v)^2}}{\overline{(T_w - T_c)^2}}, \quad (16)$$

where T_w , T_c , and T_v are the temperatures of the warm parcel ascent, control parcel ascent, and vertical-shift solution. The overbar denotes a mass-weighted mean from 150 hPa above the lowest level at which the vertical-shift

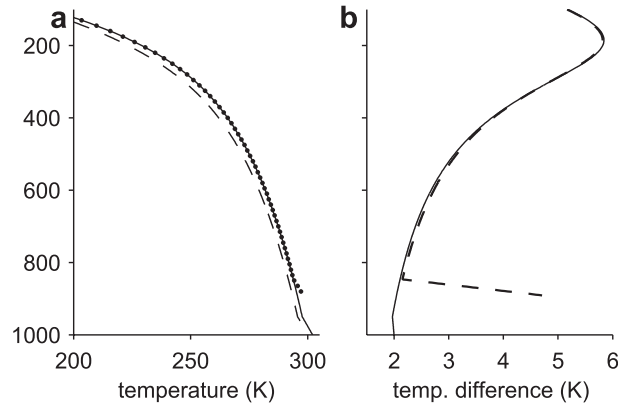


FIG. 4. (a) Pseudoadiabatic parcel ascents with surface temperatures of 300 K (dashed) and 302 K (solid), and surface relative humidity of 80% in both cases. The dotted line is an approximation of the 302-K parcel ascent calculated from the 300-K ascent using the vertical-shift transformation with $\beta = 1.122$ (corresponding to $\Delta\theta = 1.81$ K). Each adiabat is sampled at 1-hPa intervals, and the transformation is calculated by linear interpolation of the control parcel in pressure. (b) The temperature difference between the 300- and 302-K parcel ascents (solid) and the difference calculated from the transformation (dashed).

solution is well defined to the top of the atmosphere. (The value of β is insensitive to the precise choice of levels used to evaluate it.) The value of $\Delta\theta$ is calculated using (11) with the value of $T\theta$ evaluated at 600 hPa.

Apart from the dry adiabatic region of the profile below the lifted condensation level (LCL),⁵ the vertical-shift transformation is able to reproduce the temperature change remarkably well (Fig. 4). The minimized value of the error E [defined by (16)] is 0.7%. The minimized value of E is much greater (9%) if a pure upward shift in temperature is used instead of the full vertical-shift transformation (i.e., if only the parameter β is used and $\Delta\theta$ is set to zero). This shows that it is the precise combination of β and $\Delta\theta$ given by the transformation itself that allows for such a close agreement; a pure upward shift in temperature performs over 10 times worse. The value of $\beta = 1.122$ found from the least squares minimization is larger than the value of $\beta \approx 1.08$ implied by the approximate relation between β and the near-surface temperature change found earlier (15). But, if a lapse rate of 4 K km^{-1} is used in the evaluation of (14) (closer to the actual lapse rate of the parcel ascents above the dry adiabatic layer), a value of $\beta \approx 1.11$ is obtained, which is in better agreement with the result of the least squares minimization.

⁵ The mismatch at low levels results from the use of a constant surface relative humidity for both parcels, which implies that the LCL does not shift upward in accord with the transformation.

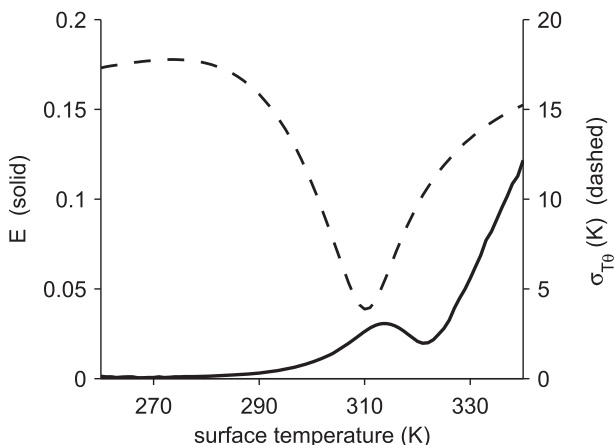


FIG. 5. Solid line (left ordinate) shows minimized error function, E , defined by (16) as a function of control parcel surface temperature. Dashed line (right ordinate) shows standard deviation of $(T\theta)^{1/2}$ over the same pressure range used to calculate E .

We next quantify the temperature dependence of the accuracy of the transformation by repeating the procedure used to create Fig. 4 for a range of surface temperatures of the control parcel. In each case, the vertical-shift transformation is applied to the control parcel ascent so as to estimate the temperature profile of a parcel ascent with a surface temperature 2 K higher and the same surface relative humidity (80%). The magnitude of vertical variation in $T\theta$ is measured here by the standard deviation,

$$s_{T\theta} = \left\{ \left[\overline{(T\theta)^{1/2} - (T\theta)^{1/2}} \right]^2 \right\}^{1/2},$$

where the overbar denotes the same mass-weighted mean used to determine β . The transformation is very accurate for low surface temperatures (Fig. 5), which makes sense given that it is exact in the limit of dry adiabatic ascent. The error E increases as the surface temperature increases, up to ~ 315 K, dropping to a local minimum at 322 K. At around these temperatures $T\theta$ becomes close to constant in the vertical—the value of $s_{T\theta}$ reaches a minimum at 312 K. At higher temperatures, the error E grows rapidly with temperature and the fidelity of the transformation breaks down, reflecting the inaccuracy of the assumption of constant $T\theta$ and the greater importance of latent heating at higher temperatures. Over the range of typical earthlike surface temperatures, however, the vertical-shift transformation performs well in reproducing the warm ascents, and the error E is typically below 2%. It will be shown in the following section that the errors introduced by mismatches in the boundary conditions are likely to be more important

than the errors related to the transformation of latent heating that have been quantified in this section.

4. Idealized general circulation model

We next discuss atmospheric GCM simulations in which we test the ability of the transformation to capture changes in the distributions of temperature, moisture, and winds as the surface temperature is increased. To focus on the dynamical accuracy of the transformation, we use a “radiation scheme” in which the radiative cooling of the atmosphere conforms to the vertical-shift transformation by depending primarily on the local specific humidity; GCMs with more realistic treatments of radiative transfer are discussed in section 5.

a. Model configuration

The idealized general circulation model is based on a version of the dynamical core of the Geophysical Fluid Dynamics Laboratory Flexible Modeling System with spectral dynamics run at T42 resolution in the horizontal and 30 levels in the vertical. Several aspects of the model formulation are similar to that of Frierson et al. (2006) and O’Gorman and Schneider (2008), but with different surface boundary conditions and a different radiation scheme. We use the simplified quasi-equilibrium moist convection scheme of Frierson (2007), a large-scale condensation scheme to prevent gridbox supersaturation, and boundary layer parameterizations similar to that of Frierson et al. (2006) [see O’Gorman and Schneider (2008) for precise details]. Note that the convective and boundary layer parameterizations do not respect the moist primitive equations used to derive the vertical-shift transformation, and it is not obvious a priori to what extent the transformation will be applicable in regions where convective or boundary layer tendencies are strong.

Our control simulation has a fixed and zonally symmetric SST distribution given by

$$T_s = T_0 + \Delta_h \left(\frac{1}{3} - \sin^2 \phi \right), \quad (17)$$

with $T_0 = 290$ K and $\Delta_h = 30$ K. The radiative tendency depends primarily on the specific humidity q as follows:

$$Q_{\text{rad}} = \begin{cases} -Q_0, & q > q_0 \\ -(T - T_{\text{strat}})/\tau, & q < q_0, \end{cases} \quad (18)$$

where $q_0 = 0.01$ g kg $^{-1}$, $Q_0 = 1$ K day $^{-1}$, $T_{\text{strat}} = 200$ K, and $\tau = 40$ days. The radiative cooling rate is constant in the troposphere (for specific humidities above q_0 , corresponding to saturation at a temperature of around 200 K for a pressure of 200 hPa) and involves a relaxation

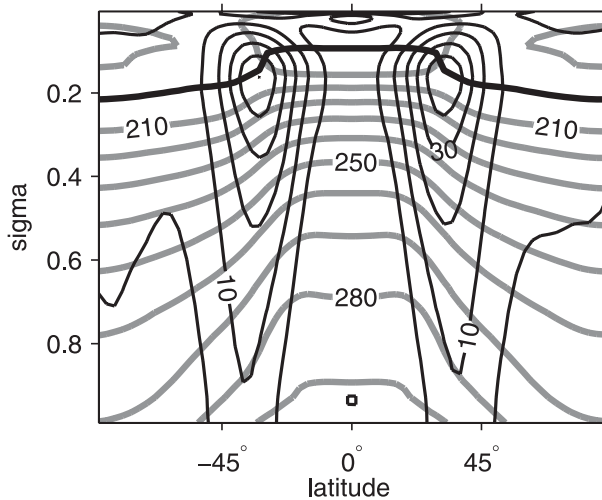


FIG. 6. Mean state of the control simulation conducted using the idealized GCM described in the text. The zonal wind (black, contour interval 10 m s^{-1}) and temperature (gray, contour interval 10 K) are shown. The tropopause (thick line) is defined as the level at which the mean lapse rate is equal to 2 K km^{-1} .

to a constant temperature in the stratosphere (for specific humidities below q_0). The form of the imposed radiative cooling ensures that, if the temperature and relative humidity transform according to the vertical-shift transformation, then so will the tropospheric radiative cooling. The stratospheric relaxation does not conform exactly to the transformation but is required to ensure stability of the simulation. The radiative tendencies (18) tend to give a tropopause near a temperature of 200 K , and this should be taken into account when interpreting upward shifts near the tropopause.

In addition to the control simulation, we also ran a warm simulation with the SST uniformly increased by 2 K . After a spinup period, zonal- and time-mean statistics were calculated over 3600 days in each simulation. The mean state of the control simulation (Fig. 6) has a single jet in each hemisphere. The strength of the Hadley cells and the global-mean precipitation rate are within a factor of 2 of those in the annual mean of the earth's current climate.

b. Results

The transformation is applied to zonal- and time-mean variables of the control simulation so as to predict the simulated response to a uniform 2 K increase in surface temperature. The value of β is chosen by minimizing an error function similar to that used for the parcel ascents and defined by (16). In this case, T_w and T_c correspond to the zonal- and time-mean temperatures of the warm and control simulation, respectively, while T_v is the temperature obtained from the application

of the vertical-shift transformation to the temperatures in the control simulation. The mass-weighted mean is taken over all latitudes and all levels above $\sigma = 0.6$.⁶ The value of $\Delta\theta$ is calculated using (11) and the global mean of $T\theta$ at $\sigma = 0.6$. These transformation parameters are then used to calculate the transformed values for all other variables. As a result, the magnitude of the upward shift is determined using the simulated change in temperature, but it is independent of the simulated changes in other variables. The values of $(\beta - 1)/\delta T_s$ and $\Delta\theta/\delta T_s$ found using this procedure are 0.05 K^{-1} [roughly consistent with (15)] and 0.69 , respectively. Here $\delta T_s = 2 \text{ K}$ is the change in global-mean SST between the control and warm simulations.

The transformation requires that fractional variations in $T\theta$ are small in order for latent heating to transform correctly. In applying the transformation to GCM simulations, both vertical and horizontal variations in $T\theta$ must be considered. The surface temperature varies by 30 K between equator and pole in the simulation described here, implying a nonnegligible fractional variation in $T\theta$ of roughly 0.2 . But, latent heating is most important in the tropics where meridional temperature gradients are relatively small; thus the errors induced by this approximation may not be very significant.

Differences in zonal- and time-mean temperature, lapse rate, relative humidity, and meridional mass streamfunction between the control and warm simulations are shown in Fig. 7 (lhs). The rhs shows the same differences estimated from the control climatology using the vertical-shift transformation. Given its simplicity, the vertical-shift transformation performs surprisingly well in emulating the response to a uniform increase in SST. The response of the temperature distribution is relatively well captured in the tropics and polar regions, although the warming in the upper troposphere is too strong in midlatitudes (Fig. 7a). The inability to precisely capture the midlatitude temperature response may be a result of a different value of β being appropriate there; in the appendix, it is shown that the temperature response is captured with considerable fidelity at all latitudes if β is allowed to vary with latitude. The improvement afforded by allowing β to vary is less pronounced for other variables, however, and the validity of the transformed solution as a solution to the governing equations is reduced. We continue to analyze results using a single value of β globally, noting that the

⁶ The lower level used in the calculation of β is chosen to be above the region of the atmosphere in which the transformed solution refers to regions with substantial boundary layer temperature tendencies in the original solution (see hatching in Fig. 7). The value of β obtained is insensitive to the precise choice of lower level used.

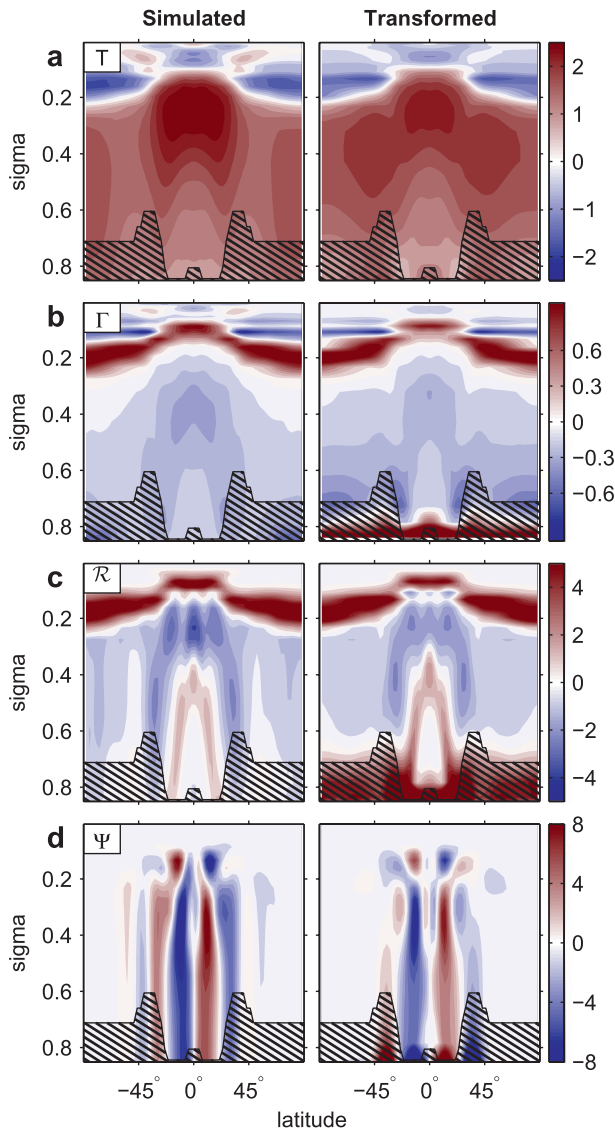


FIG. 7. Normalized differences (left) between the control and warm simulations and (right) calculated using the vertical-shift transformation. Changes in zonal- and time-mean (a) temperature (K), (b) lapse rate (K km^{-1}), (c) relative humidity (%), and (d) meridional mass streamfunction (10^9 kg s^{-1}), all normalized by the change in SST between simulations (2 K). The hatching shows where the vertical-shift transformation may refer to regions in the control simulation with substantial boundary layer tendencies (see text). Interhemispheric asymmetries are indicative of sampling error.

transformation then involves only a single tunable parameter while describing changes to the entire general circulation.

The changes in temperature lapse rate are shown in Fig. 7b and are well captured except in the lower troposphere at high latitudes. The increase in tropopause height is also captured, although some of this may be directly attributable to the constraint on tropopause

height imposed by the specified dependence of radiative cooling on specific humidity. The transformation does not capture the lapse-rate response close to the boundary below which the transformed solution is no longer well defined ($\sigma = 1/\beta$). As discussed in section 2e, this is to be expected because of the effects of boundary layer processes; the regions marked with hatching in Fig. 7 give an indication of where the transformed solution refers to regions in the control simulation with substantial parameterized boundary layer tendencies of temperature. The region of substantial boundary layer tendencies in the control simulation is taken to extend to the highest level at which the magnitude of the mean temperature tendencies from the boundary layer scheme are above 10^{-6} K s^{-1} (roughly one-tenth of their maximum value).

The transformation also captures much of the simulated response of relative humidity, both in the overall structure and, to a lesser degree, in magnitude, including a complicated pattern of increases and decreases in equatorial and subtropical regions (Fig. 7c). As for the lapse rate, the errors in the transformation largely occur in the lower part of the troposphere, and much of the disagreement is confined to regions influenced by strong boundary layer tendencies.

Changes in the meridional mass streamfunction also show similarities in the simulated and transformed responses. In both cases there is a decrease in strength of both Hadley and Ferrel cells over most of the troposphere, with small increases near the tropopause relating to an upward extension of the circulation. However, the quantitative changes in the streamfunction are generally less well predicted by the transformation than in the case of the relative humidity field, especially in the extratropics. Some of these differences may be a result of sampling error, as evidenced by the departure from interhemispheric symmetry of the simulated response of the mass streamfunction (since the boundary conditions are symmetric between the hemispheres). Considerable low-frequency variations in the streamfunction may be related to annular mode-like variation that is known to have long time scales in aquaplanet models (Cash et al. 2002). We measure the Hadley cell strength as the maximum in the absolute value of the zonal- and time-mean streamfunction, averaged between hemispheres. The vertical-shift transformation implies a decrease of $\sim 6\% \text{ K}^{-1}$ in Hadley cell strength relative to the change in global-mean surface air temperature, while the simulated response is considerably weaker ($\sim 3\% \text{ K}^{-1}$). The transformation also predicts a weakening of the Ferrel cell in response to surface warming, and this is indeed what occurs in the simulations, albeit at a lesser rate than given by the transformation.

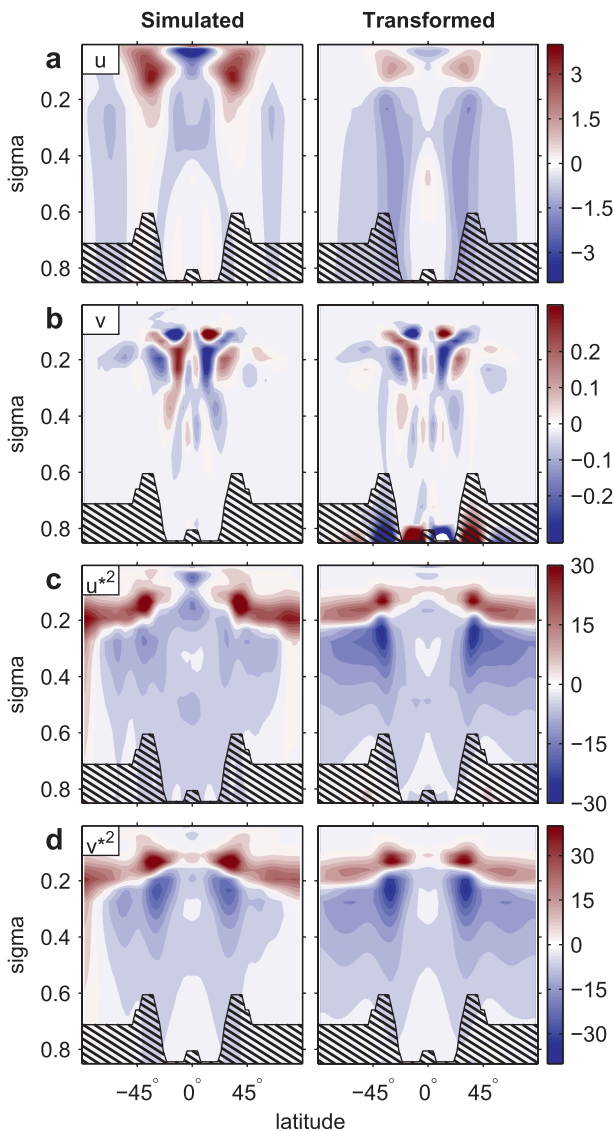


FIG. 8. As in Fig. 7, but for normalized changes in (a) zonal and (b) meridional mean winds (m s^{-1}) and (c) zonal and (d) meridional wind variances ($\text{m}^2 \text{s}^{-2}$). The variances are calculated using four-times daily data with respect to a zonal and time mean.

The vertical-shift transformation does not capture the response of the mean zonal wind (Fig. 8a). While there are some similarities in the simulated and transformed changes at upper levels, the transformation implies a decrease in the strength of the wind below the jets that is too strong and an increase above that is too weak. There are also simulated decreases in the zonal wind at high latitudes that the vertical-shift transformation does not capture. On the other hand, the response of the mean meridional wind in the idealized GCM simulations forms a complex pattern of increases and decreases in the upper troposphere that is remarkably well captured

by the vertical-shift transformation (Fig. 8b). The changes in meridional and zonal wind variances are also well described by the transformation, with increases in the upper troposphere and decreases below, and the largest changes occurring near the location of the jet (Figs. 8c,d). The decrease implied by the transformation is slightly too strong while the increase is slightly too weak, resulting in less eddy activity overall in the transformed climate than occurs in the warm simulation. The reduction in eddy activity and associated meridional fluxes of zonal momentum implied by the transformation could be thought to be consistent with the transformed reduction in lower-tropospheric mean zonal winds, although there is no requirement for the vertical-shift transformation to respect the vertically integrated zonal momentum budget in this way. Rather, the inaccuracy for the changes in zonal winds is likely related to the inability of the transformation to satisfy the surface boundary condition for zonal wind.

Overall, the extent to which the transformation reproduces the simulated changes in the idealized GCM simulations is remarkable given the simplicity of the transformation. It should also be stressed that the transformation has only one free parameter, which is fit using the global temperature response and does not depend on the response in humidity or wind fields. To summarize the results, Fig. 9 shows a Taylor diagram comparing the transformed response in each variable to the simulated response (see Taylor 2001). Standard deviations and correlation coefficients of the responses and their differences are calculated globally for levels above $\sigma = 0.6$ and with mass weighting. The standard deviations shown in the diagram are normalized by the standard deviation of the simulated response in each case. The normalized standard deviation is close to one for all variables except the mean zonal wind, which supports the existence of a coherent upward shift across variables as implied by the transformation. With the exception of the mean zonal wind, all variables have correlation coefficients greater than 0.8 and normalized errors less than roughly 0.6. The normalized error shown is the pattern root-mean-square difference (Taylor 2001) and does not include the mean bias. The mean bias is generally less than 10% of the total error.

Figures 8 and 9 show that the transformation captures less of the simulated response of the mean zonal wind as compared to other variables. The difference between the simulated and transformed responses in mean zonal wind may be decomposed into components—one associated with near-surface wind changes (which we will refer to as the barotropic component) and a baroclinic component that is primarily related to changes in horizontal temperature gradients. The baroclinic component

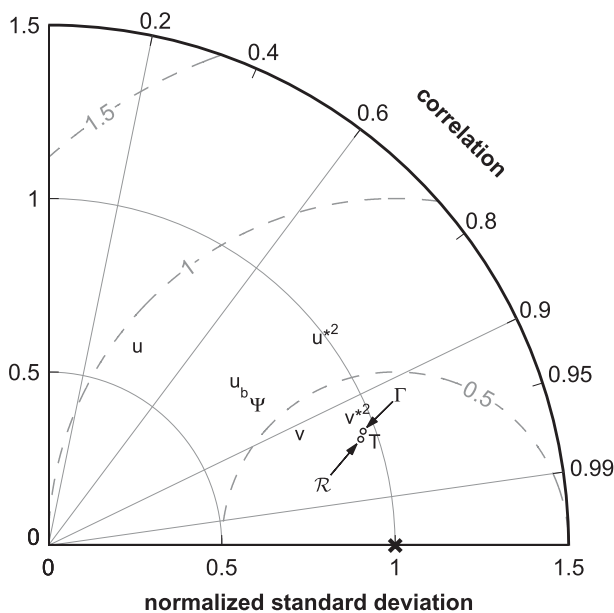


FIG. 9. Normalized Taylor diagram quantifying the degree of similarity in the zonal and time mean between the simulated and transformed patterns of response in the idealized GCM simulations for temperature (T), lapse rate (Γ), relative humidity (R), meridional mass streamfunction (Ψ), mean zonal (u) and meridional (v) winds, and zonal (u^{*2}) and meridional (v^{*2}) wind variances. The transformation of the zonal wind with a barotropic offset is shown as u_b (see text). The diagram shows the standard deviation of the transformed response normalized by the standard deviation of the simulated response (distance to origin), the correlation coefficient between the transformed and simulated response (cosine of angle to the abscissa), and the normalized error (distance to point marked “X”). The error value does not include the global-mean bias. All quantities are calculated based on averages over all latitudes and levels above $\sigma = 0.6$ with appropriate mass weighting.

may be isolated by allowing a latitude-dependent (but height independent) offset Δu to be added to the transformation to match the barotropic component of the simulated changes. Indeed, this offset could be included in the framework of the transformation using the Galilean invariance of the tangent plane equations in the zonal direction, although we do not pursue this in detail here. The fidelity of the transformation including this offset is shown by the point marked u_b in Fig. 9. The offset is calculated as the difference between the simulated and transformed mean zonal wind at each latitude and at the lowest level at which the transformation is well defined. Other definitions using multiple levels give similar results. Inclusion of the barotropic offset leads to some improvement in the match with the simulated response, but the mean zonal wind remains one of the variables most poorly captured by the transformation. In the next section we consider simulations in the CMIP3

ensemble for which the barotropic offset is found to improve the fidelity of the transformed zonal wind to be on a par with the lapse rate and relative humidity. Part of the reason for this difference may be that a poleward shift in the midlatitude jets occurs in the CMIP3 simulations (e.g., Fyfe et al. 1999; Yin 2005) but does not occur to the same extent in the idealized GCM simulations. The poleward shift cannot be captured by the vertical-shift transformation, and it increases the error that resides in the barotropic component. This is also a difference between the idealized GCM results shown here and those of Lorenz and DeWeaver (2007), who found that a poleward (and upward) shift of the jets resulted from raising the tropopause height in a dry idealized GCM.

5. Comprehensive general circulation models

We next apply the vertical-shift transformation to simulations of climate change from the third Coupled Model Intercomparison Project. We examine results from 10 fully coupled atmosphere–ocean GCMs⁷ using the period 1981–2000 of the twentieth-century simulations as the control climate and the period 2081–2100 under the forcing scenario A1b from the Special Report on Emissions Scenarios (SRESA1b) (Nakićenović and Swart 2000) as the warm climate. (An example of the application of an upward shift to the change in cloud fraction in one such model is shown in Fig. 1, although cloud fraction is not explicitly included in the transformation discussed here.) In contrast to the idealized GCM simulations, the CMIP3 simulations include realistic representations of radiative transfer and ice processes, and thus the conditions on the radiative cooling and humidity fields required for the transformation to be valid may not be satisfied. Nevertheless, we will show that a substantial portion of the response to warming in simulations with comprehensive GCMs may be described using the vertical-shift transformation with a single tunable parameter.

The vertical-shift transformation is applied individually in each climate model to zonal- and time-mean fields of

⁷ The models used are BCCR-BCM2.0, GFDL CM2.0, GFDL CM2.1, CNRM-CM3, CSIRO Mk3.5, ECHAM5, FGOALS-g1.0, INM-CM3.0, MIROC3.2(medres), and MRI CGCM2.3.2. Only the first three models are used in the calculation of ensemble-mean wind variances (Figs. 12c,d) because only these models had daily wind data available above 200 hPa; the results are similar below 200 hPa for the entire ensemble. The pressure velocity was not available for BCCR-BCM2.0 and CSIRO Mk3.5, and these models are excluded from the calculation of ensemble-mean changes in pressure velocity (Fig. 11).

the control climate to give an estimate of the general circulation in the warm climate. As in the application to the idealized GCM simulations in section 4, a value of β is found to best match the global temperature changes, and the same value of β is used to calculate the change in all other fields. The fitting procedure is the same as for the idealized GCM—the mean-squared difference between the warm-climate temperature field and that from the transformation is minimized over all latitudes and levels above the 600-hPa pressure level, and the global mean of $T\theta$ at 600 hPa is used in Eq. (11). The resulting value of $(\beta - 1)\delta T_s$ varies between 0.036 and 0.048 K^{-1} between models, with an ensemble-mean value of 0.044 K^{-1} [roughly consistent with (15)]. The associated ensemble-mean value of $\Delta\theta/\delta T_s$ is 0.59, ranging between 0.51 and 0.67 among models. Here, δT_s is the change in global-mean surface air temperature. Differences between the control and warm climate for each model are normalized by δT_s before being combined into an ensemble mean, both for the simulated differences and the differences given by the vertical-shift transformation. While we only show ensemble-mean quantities, the vertical-shift transformation has a similar level of accuracy when applied to climate change in individual model simulations.

a. Temperature and moisture

The temperature change implied by the transformation compares well with the simulated temperature change (Fig. 10a), although, as in the case of the idealized GCM, there is too much warming in the mid-latitude troposphere. The ability of the transformation to capture the vertical structure of the changes in the mid- and upper troposphere is also clearly demonstrated for the lapse rate changes (Fig. 10b). The ability to capture the large lapse rate changes associated with the increase in tropopause height is notable given that realistic radiative transfer is used in these models (unlike in the idealized GCM in which the radiative cooling was prescribed to shift upward with specific humidity). Lorenz and DeWeaver (2007) reported similar results for the lapse rate changes in CMIP3 models but with a focus on the tropopause region and using a pure upward shift for temperature that does not capture the changes in the midtropospheric lapse rate.

The vertical-shift transformation captures changes in relative humidity associated with the increase in tropopause height, as well as decreases in relative humidity in the tropical upper troposphere and subtropics (Fig. 10c). Sherwood et al. (2010) also showed that upward shifts account for a significant part of the relative humidity response in CMIP3 models, including different responses

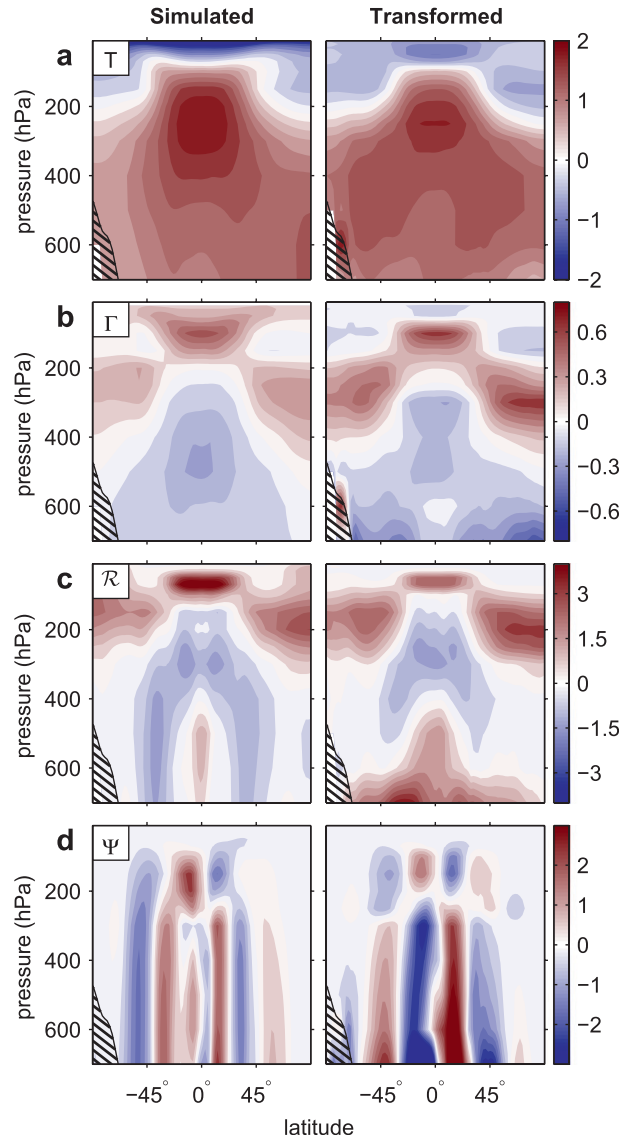


FIG. 10. Ensemble mean of the normalized changes in zonal- and time-mean variables between the twentieth-century simulation (1981–2000) and the SRESA1b scenario (2081–2100) in CMIP3 models. (left) Simulated changes and (right) changes calculated from the vertical-shift transformation for (a) temperature (K), (b) lapse rate (K km^{-1}), (c) relative humidity (%), and (d) meridional mass streamfunction (10^9 kg s^{-1}), all normalized by the change in global-mean surface air temperature (K) prior to taking the ensemble mean. Hatching indicates regions in which boundary effects are likely to be important (see text).

in different models because of their different climatologies of mean relative humidity.

The vertical-shift transformation is much less accurate in reproducing lower-tropospheric changes in lapse rates and relative humidities. Figure 10 only shows changes above 700 hPa since, as discussed previously, the transformation breaks down in the boundary layer.

The lowest level at which the transformation may be applied is taken to be

$$p_b = (p_s - \Delta p_{BL})/\beta,$$

where $\Delta p_{BL} = 150$ hPa is a nominal boundary layer thickness. At most latitudes p_b is somewhat greater than 700 hPa, except in the Antarctic, where hatching is used to indicate regions that are beneath the pressure level p_b . Despite this accommodation of a 150-hPa boundary layer, the vertical-shift transformation disagrees strongly with the simulated changes in levels just above 700 hPa. This could be an indication that boundary layer fluxes are significant at levels higher than 150 hPa above the surface, or it could, for example, be an effect of parameterized convection.

b. Winds

Changes in the meridional mass streamfunction are less well captured than changes in thermodynamic and moisture variables (Fig. 10d). While the pattern of increases and decreases is largely correct in the Northern Hemisphere and near the tropopause of both hemispheres, the Southern Hemisphere troposphere is dominated by meridional shifts and the magnitude of the changes in the transformed solution is too strong by at least a factor of 2 in both hemispheres. Qualitatively, the weakening in tropical overturning in the model simulations is captured by the transformation, but the maximum absolute value of the meridional mass streamfunction averaged between hemispheres decreases by $\sim 5\% \text{ K}^{-1}$ according to the transformation, while the model simulations have decreases in the range $0.5\text{--}1.5 (\% \text{ K}^{-1})$. In the midlatitudes, the changes in the overall strength of the Eulerian-mean overturning are not captured by the transformation, with the streamfunction maximum poleward of 30° latitude decreasing by $\sim 4\% \text{ K}^{-1}$ according to the transformation, but not changing or increasing slightly in the simulations.

The zonal-mean pressure velocity (whose changes may be inferred from Fig. 10d) represents only a small residual of larger pressure velocities in ascent and descent regions distributed around the globe, as demonstrated in Fig. 11a. Previous studies have found that the zonally symmetric circulation weakens less than the zonally asymmetric circulation (e.g., Vecchi and Soden 2007), a difference that is not captured by the vertical-shift transformation. To examine the zonally asymmetric response, we apply the vertical-shift transformation to the pressure velocity at 500 hPa at each latitude and longitude. Both the simulated response and the response given by the vertical-shift transformation tend to be of opposite sign to the climatological value (Figs. 11b,c),

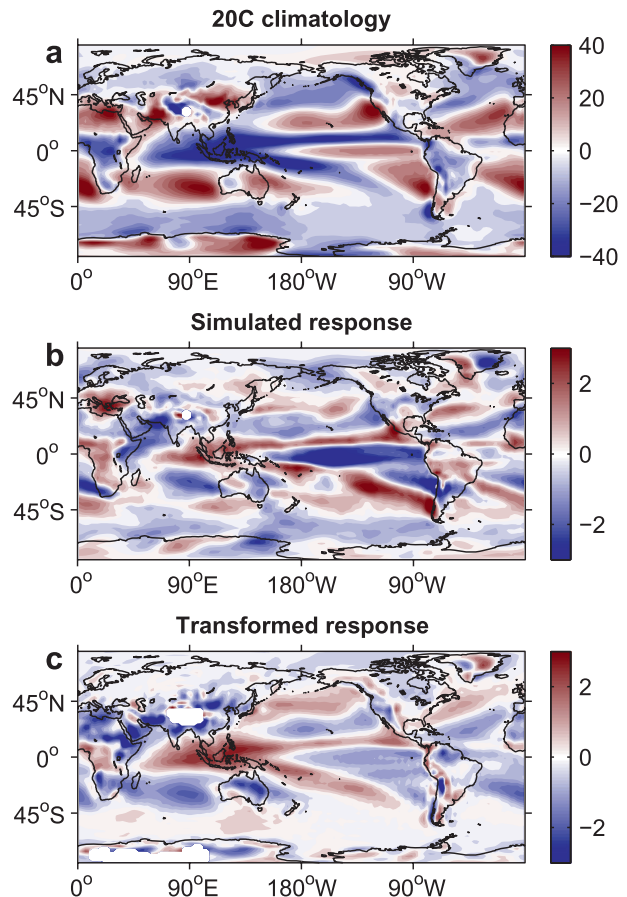


FIG. 11. Global map of the CMIP3 ensemble- and time-mean pressure velocity (hPa day^{-1}) at 500 hPa: (a) twentieth-century climatology (1981–2000), (b) response under the SRESA1b scenario and (c) response calculated using the vertical-shift transformation and the twentieth-century climatology. For (b) and (c) individual model changes are normalized by the global-mean change in surface air temperature before being combined into the ensemble mean.

implying a reduction in overturning in most places. The largest changes are in the equatorial Pacific, where both the simulated response and the transformation show less ascent over the Maritime Continent and more in the central and eastern Pacific. Similarly, the sign of the simulated response over the Pacific Ocean, Indian Ocean, and Africa is correctly captured by the transformation. There are some quantitative differences between the transformation and simulated changes. For instance, the simulated response shows stronger increases in ascent in the eastern tropical Pacific than decreases in the west [related to the tendency for coupled climate models to simulate a more “El Niño-like” state in a warmer climate (e.g., Vecchi and Soden 2007)], whereas the transformation gives the opposite. Thus, the response of the transformation for the pressure velocity is not quantitatively

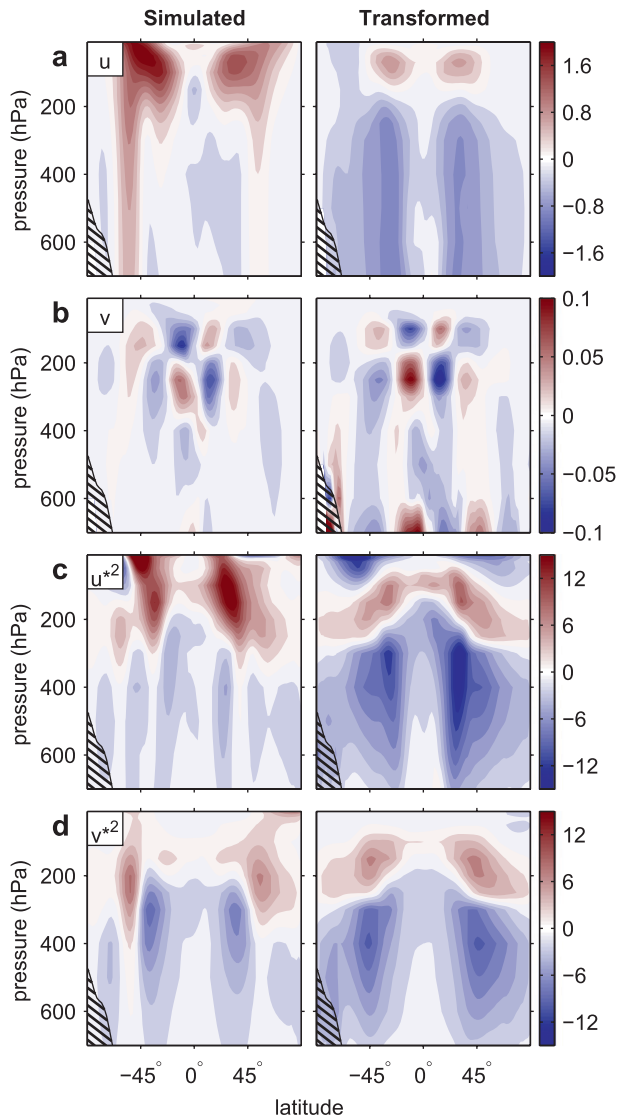


FIG. 12. As in Fig. 10, but for normalized changes in (a) mean zonal wind (m s^{-1}), (b) mean meridional wind (m s^{-1}), (c) zonal wind variance ($\text{m}^2 \text{s}^{-2}$), and (d) meridional wind variance ($\text{m}^2 \text{s}^{-2}$). Wind variances are calculated based on daily data with respect to the time-mean before being zonally averaged.

accurate, but the agreement is better than might be inferred from consideration of the changes in meridional mass streamfunction alone.

There are considerable differences in the simulated response of the mean zonal wind and the response given by the vertical-shift transformation (Fig. 12a). The transformation shows a pronounced decrease in the troposphere with an increase near the tropopause, while the simulated changes show a larger increase near the tropopause and little change in most of the troposphere. The vertical-shift transformation appears to reproduce the pattern of simulated changes in the mean and variance of

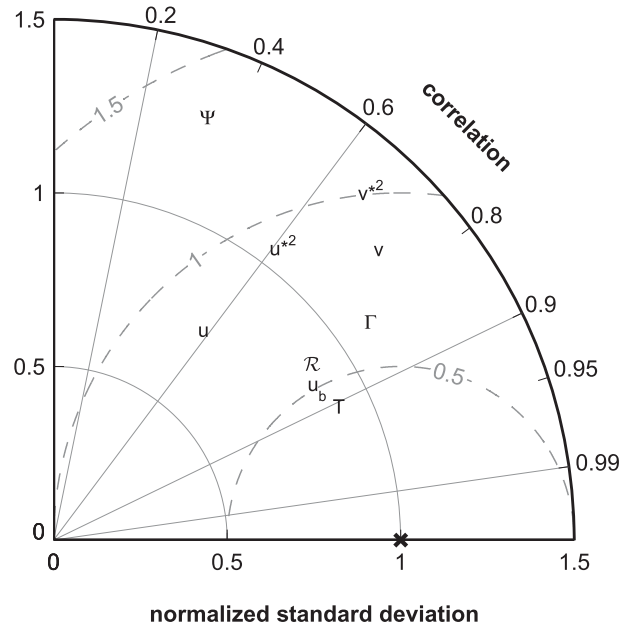


FIG. 13. As in Fig. 9, but for the ensemble mean of the CMIP3 simulations with quantities calculated based on averages over all latitudes and pressures above 600 hPa.

the meridional wind better than those of the zonal wind, although the magnitudes of the changes are not captured. Both the simulated response and transformation show increases in wind variance near the tropopause at midlatitudes, and decreases below. But the decreases in wind variance in the troposphere are too large in the vertical-shift transformation, and the simulated response also exhibits a poleward shift (especially for the meridional wind variance).

c. Summary and poleward shift

The extent to which the transformation captures the simulated changes in the CMIP3 ensemble is summarized by the Taylor diagram shown in Fig. 13. Correlation coefficients are above 0.8 and normalized errors are below roughly 0.6 for temperature, lapse rate, and relative humidity. The dynamical variables, on the other hand, have lower correlation coefficients and normalized errors close to unity. The normalized error is considerably greater than unity for the meridional mass streamfunction, indicating that by this measure the transformation is less accurate than simply assuming no change.

The pattern of mismatch in the response of the mean zonal wind (Fig. 12) suggests that the difference between the simulated and transformed responses in the mean zonal wind is largely in the barotropic component, and thus related to the inability of the transformation to satisfy the surface boundary conditions for momentum (the transformation implies a general weakening of surface

winds), together with a poleward shift of the jets that the vertical-shift transformation does not capture.⁸ Note that the poleward shift does not account for all of the barotropic component of the error, and there is considerable weakening of the midlatitude jets in the transformation that is not reflected in the model simulations. When a latitude-dependent barotropic offset is included in the transformation of the zonal wind (see section 4), the level of agreement improves considerably, as shown by the symbol u_b in Fig. 13.

In general, the vertical-shift transformation is less accurate in reproducing the response to warming in the CMIP3 simulations compared with the idealized GCM simulations, especially for the winds. This is not surprising given that the assumption of a simple upward shift in the radiative tendencies with warming is less accurate, given that the more complicated forcing implies a more complex response, and given that a poleward shift of the circulation occurs to a greater extent. Despite these caveats, the transformation still captures a number of the major features of the simulated climate changes in the mid- and upper troposphere in both the tropics and midlatitudes of the CMIP3 simulations.

6. Conclusions

We have examined the extent to which changes in temperature, humidity, and circulation that occur under global warming may be understood in terms of a vertical shift. Using the inviscid moist primitive equations on the sphere, a one-parameter transformation was derived that allows for a warming atmosphere and that shifts the circulation upward in a manner consistent with the governing equations. While all variables are shifted upward by the transformation, the pressure velocity also decreases in magnitude and the change in temperature includes an additional offset. Because of the effects of latent heat release, the transformation is only accurate to the extent that fractional variations in $T\theta$ are small. For earthlike climates this condition is approximately satisfied in the troposphere, especially in the tropical lower troposphere where latent heating is most important.

The transformation was shown to be accurate in reproducing moist-adiabatic parcel ascents as the surface temperature was varied. This constitutes a simple but nontrivial demonstration that the transformation is able to reproduce changes to the mean temperature

structure of an idealized convecting atmosphere. The transformation was evaluated in a more general framework using simulations with both an idealized GCM and an ensemble of comprehensive GCMs. The radiative cooling parameterization in the idealized GCM was constructed so as to conform to the transformation, and the transformation was found to perform well in reproducing changes in the mean thermodynamic and moisture distributions and in the meridional wind and wind variances. For the comprehensive GCM simulations, the similarity between the simulated and transformed responses was less pronounced than in the idealized GCM simulations (possibly related to the radiative cooling not simply shifting upward and a greater poleward shift of the winds in the midlatitudes), but some of the important features of the thermodynamic and dynamic responses were still captured.

According to the transformation, the pressure velocity decreases in magnitude as it shifts upward, implying a decrease in the strength of the mass overturning of the atmosphere in proportion to the transformation parameter β . For typical values of β found in the tropics of the idealized and comprehensive GCM simulations, this corresponds to a decrease in overturning of 4–6 (% K^{-1}) relative to the change in global-mean surface air temperature. Further work would be needed to establish the relevance of the rate of change in overturning given by the transformation. One important limitation is that the transformation does not account for the radiative effects of well-mixed greenhouse gases or absorbing aerosols that could also affect global-mean precipitation and overturning (e.g., O’Gorman et al. 2012).

Mismatches between the transformation and the simulated response to climate change were primarily either in or near the boundary layer (as in the case of the relative humidity) or dynamically related to an inability to satisfy the correct surface boundary conditions (as in the case of the zonal wind). In light of this, it may be useful to decompose the response of the general circulation into the sum of two parts: the upward shift outlined here and a correction to account for mismatches in surface boundary conditions. We speculate that it may be possible to reproduce the correction by simulating the climate response to a change in boundary conditions from the usual boundary conditions to the boundary conditions that the transformed solution would satisfy. The correction might only be large close to the surface for some variables (e.g., relative humidity), but could be expected to have a barotropic component in the case of the zonal wind.

Because the transformation of temperature is not purely an upward shift [due to the $\Delta\theta$ term in (13e)], the transformation implies that both the cold-point temperature and the divergence-weighted temperature in

⁸ A complication regarding the poleward shift is the inconsistent treatment of ozone recovery between models (Son et al. 2008). However, we find similar results when only models with no changes in ozone over the twenty-first century are considered.

the tropical upper troposphere should decrease with surface warming. The latter quantity has recently been investigated by Zelinka and Hartmann (2010), who found that in the CMIP3 models the tropical-mean divergence-weighted temperature increases as the climate warms, although much less so than the surface temperature. This discrepancy may indicate that the assumption of a simple upward shift of the radiative cooling is not sufficient to capture such relatively subtle changes in this region of the tropical atmosphere. Nevertheless, the vertical-shift transformation accurately reproduces much of the simulated changes in the lapse rate of the tropical troposphere as the climate warms. A simple upward shift was also found to reproduce much of the change in mean cloud fraction in a simulation of greenhouse-gas-driven warming (cf. Fig. 1), and it would be worthwhile to try to extend the vertical-shift transformation to include such cloud properties.

The transformation introduced here provides a simple framework in which to analyze the upward shift of the general circulation under global warming. It offers the advantage that it is based on the governing equations, and it suggests that the upward shift is a coherent response of the circulation of the mid- and upper troposphere, rather than something that occurs in one or two variables in a particular region. The extent to which the transformation (with a single tunable parameter) captures the global response of the circulation under a given radiative forcing may be expected to depend on the complexity of the forcing and the extent to which the circulation also shifts meridionally. Given that different climate models generate different control climatologies, the transformation may be helpful for understanding the source of intermodel scatter in the simulated response to climate change (cf. Sherwood et al. 2010), and this is left to future work.

Acknowledgments. The authors acknowledge the modeling groups, the Program for Climate Model Diagnosis and Intercomparison, and the World Climate Research Programme Working Group on Coupled Modeling for their roles in making available the CMIP3 multimodel dataset. Support for this dataset is provided by the Office of Science, U.S. Department of Energy. This work was partially supported by NSF Grant AGS-1148594. Two anonymous reviewers provided helpful comments on this manuscript.

APPENDIX

Alternative Calculation of the Transformation: Meridionally Varying β

The derivation in section 2 assumes that the transformation parameter β is constant in both space and

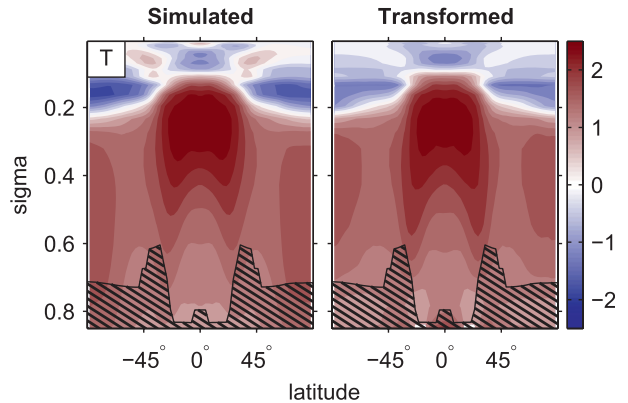


FIG. A1. As in Fig. 7a, but with the transformation parameter β allowed to vary with latitude. The values of β vary between 1.08 and 1.12 depending on latitude and were calculated by minimizing the error function (16) at each latitude independently.

time. Consistently, we have used a single global value of β when applying the transformation to simulations of climate change. However, β could be allowed to vary with latitude such that the transformed solution still remains an approximate solution to the governing equation if the variations in β are small enough. Figure A1 shows an application of the transformation to the idealized GCM simulations in which β is allowed to vary with latitude. The value of β is calculated by minimizing the error function (16) at each latitude independently, and a corresponding value of $\Delta\theta$ was then determined at each latitude using (11). The extent to which the simulated response is captured by the transformation is improved considerably in the case of temperature (cf. Fig. 7a), especially in the subtropics, but less so for other variables (not shown).

To quantify the extent to which β should be allowed to vary with latitude, consider the example of the transformation of the meridional gradient of the zonal wind,

$$\frac{\partial u'}{\partial \phi} = \frac{\partial u}{\partial \phi} \Big|_{\beta p} + \frac{\partial \beta}{\partial \phi} p \frac{\partial u}{\partial p} \Big|_{\beta p}, \quad (\text{A1})$$

where u' is the transformed solution. The difference in this quantity between the control and vertically shifted solution is approximately given by

$$\frac{\partial(u' - u)}{\partial \phi} = p \left[(\beta - 1) \frac{\partial^2 u}{\partial \phi \partial p} \Big|_p + \frac{\partial \beta}{\partial \phi} \frac{\partial u}{\partial p} \Big|_{\beta p} \right]. \quad (\text{A2})$$

For the change between the control and vertically shifted solution to be accurate, the second term on the right-hand side of the above equation must be small compared with the first term on the right-hand side. If meridional

variations in $\partial_p u$ and β occur on similar length scales, then this condition is reduced to requiring that the meridional variation $\Delta\beta$ satisfies

$$\frac{\Delta\beta}{\beta - 1} \ll 1. \quad (\text{A3})$$

For the application of the transformation in Fig. A1, $(\beta - 1)/\delta T \approx 0.05$, varying between a maximum of 0.058 in the tropics and 0.038 in the midlatitudes. This yields $\Delta\beta/(\beta - 1) \approx 0.4$, implying that allowing β to vary may introduce substantial errors. However, there are some regions of the atmosphere, such as the tropics where β is indeed relatively constant, and the solution will be valid locally in these regions. Allowing β to vary for the CMIP3 models also leads to a greater similarity between the transformed and simulated temperature responses, but the condition (A3) is still not very well satisfied with $\Delta\beta/(\beta - 1) \approx 0.5$.

REFERENCES

- Cash, B. A., P. J. Kushner, and G. K. Vallis, 2002: The structure and composition of the annular modes in an aquaplanet general circulation model. *J. Atmos. Sci.*, **59**, 3399–3414.
- Dopplnick, T. G., 1972: Radiative heating of the global atmosphere. *J. Atmos. Sci.*, **29**, 1278–1294.
- Frierson, D. M. W., 2007: The dynamics of idealized convection schemes and their effect on the zonally averaged tropical circulation. *J. Atmos. Sci.*, **64**, 1959–1976.
- , I. M. Held, and P. Zurita-Gotor, 2006: A gray-radiation aquaplanet moist GCM. Part I: Static stability and eddy scale. *J. Atmos. Sci.*, **63**, 2548–2566.
- Fyfe, J. C., G. J. Boer, and G. M. Flato, 1999: The Arctic and Antarctic oscillations and their projected changes under global warming. *Geophys. Res. Lett.*, **26**, 1601–1604.
- Garner, S. T., D. M. W. Frierson, I. M. Held, O. Pauluis, and G. K. Vallis, 2007: Resolving convection in a global hypohydrostatic model. *J. Atmos. Sci.*, **64**, 2061–2075.
- Hartmann, D. L., and K. Larson, 2002: An important constraint on tropical cloud-climate feedback. *Geophys. Res. Lett.*, **29**, 1951, doi:10.1029/2002GL015835.
- , J. R. Holton, and Q. Fu, 2001: The heat balance of the tropical tropopause, cirrus, and stratospheric dehydration. *Geophys. Res. Lett.*, **28**, 1969–1972.
- Held, I. M., and B. J. Soden, 2006: Robust responses of the hydrological cycle to global warming. *J. Climate*, **19**, 5686–5699.
- Ingram, W., 2010: A very simple model for the water vapour feedback on climate change. *Quart. J. Roy. Meteor. Soc.*, **136**, 30–40.
- Knutson, T. R., and S. Manabe, 1995: Time-mean response over the tropical Pacific to increased CO₂ in a coupled ocean–atmosphere model. *J. Climate*, **8**, 2181–2199.
- Kuang, Z., and D. L. Hartmann, 2007: Testing the fixed anvil temperature hypothesis in a cloud-resolving model. *J. Climate*, **20**, 2051–2057.
- Kushner, P. J., I. M. Held, and T. L. Delworth, 2001: Southern Hemisphere atmospheric circulation response to global warming. *J. Climate*, **14**, 2238–2249.
- Lorenz, D. J., and E. T. DeWeaver, 2007: Tropopause height and zonal wind response to global warming in the IPCC scenario integrations. *J. Geophys. Res.*, **112**, D10119, doi:10.1029/2006JD008087.
- Merlis, T. M., and T. Schneider, 2011: Changes in zonal surface temperature gradients and Walker circulations in a wide range of climates. *J. Climate*, **24**, 4757–4768.
- Mitchell, J., and W. Ingram, 1992: Carbon dioxide and climate: Mechanisms of changes in cloud. *J. Climate*, **5**, 5–21.
- Muller, C. J., P. A. O’Gorman, and L. E. Back, 2011: Intensification of precipitation extremes with warming in a cloud-resolving model. *J. Climate*, **24**, 2784–2800.
- Nakićenović, N., and R. Swart, Eds., 2000: *Special Report on Emissions Scenarios*. Cambridge University Press, 599 pp.
- O’Gorman, P. A., and T. Schneider, 2008: The hydrological cycle over a wide range of climates simulated with an idealized GCM. *J. Climate*, **21**, 3815–3832.
- , R. P. Allan, M. P. Byrne, and M. Previdi, 2012: Energetic constraints on precipitation under climate change. *Surv. Geophys.*, **33**, 585–608.
- Schneider, T., P. A. O’Gorman, and X. J. Levine, 2010: Water vapor and the dynamics of climate changes. *Rev. Geophys.*, **48**, RG3001, doi:10.1029/2009RG000302.
- Sherwood, S. C., W. Ingram, Y. Tsushima, M. Satoh, M. Roberts, P. L. Vidale, and P. A. O’Gorman, 2010: Relative humidity changes in a warmer climate. *J. Geophys. Res.*, **115**, D09104, doi:10.1029/2009JD012585.
- Son, S.-W., and Coauthors, 2008: The impact of stratospheric ozone recovery on the Southern Hemisphere westerly jet. *Science*, **320**, 1486–1489.
- Taylor, K., 2001: Summarizing multiple aspects of model performance in a single diagram. *J. Geophys. Res.*, **106** (D7), 7183–7192.
- Tompkins, A. M., and G. C. Craig, 1999: Sensitivity of tropical convection to sea surface temperature in the absence of large-scale flow. *J. Climate*, **12**, 462–476.
- Vecchi, G. A., and B. J. Soden, 2007: Global warming and the weakening of the tropical circulation. *J. Climate*, **20**, 4316–4340.
- Yin, J. H., 2005: A consistent poleward shift of the storm tracks in simulations of 21st century climate. *Geophys. Res. Lett.*, **32**, L18701, doi:10.1029/2005GL023684.
- Zelinka, M. D., and D. L. Hartmann, 2010: Why is longwave cloud feedback positive? *J. Geophys. Res.*, **115**, D16117, doi:10.1029/2010JD013817.